B. M.D. Hidayathulla Khan*, V. Ramachandra Prasad, and R. Bhuvana Vijaya

Thermal Radiation on Mixed Convective Flow in a Porous Cavity: Numerical Simulation

https://doi.org/10.1515/nleng-2017-0053
Received April 24, 2017; revised September 21, 2017; accepted January 20, 2018.

Abstract: In this paper, the influence of mixed convection in a porous square enclosure under the effect of radiation is numerically examined. The top and bottom walls are maintained at uniform temperature θ_c while some portion of the vertical walls is partially heated with temperature θ_h and rest of the vertical walls are thermally insulated, with $\theta_h > \theta_c$. The non-dimensional governing equations are solved by MAC (Marker and Cell) method. The effect of various parameters (thermal Grashof number, Darcy number, Prandtl number, Reynolds number) on flow patterns and heat transfer has been presented.

Keywords: Mixed Convection; Square Enclosure; Darcy Porous Medium; Thermal Radiation; Heat Source

1 Introduction

Over the past few decades, several researchers studied convection in lid driven cavities with different thermal boundary conditions. Literature review guarantees that many researchers have analysed convective heat transfer in porous cavity play a vital role in various fields such as cooling of microprocessors and electronic components, nuclear waste, geothermal systems, drying of food grains and textile materials, chemical industries, biological processes and many others. Mixed convection is the combination of forced and natural convection. Many researchers [1–6, 6] studied mixed convection within enclosures. Kalla et al. [7] adopted the Boussinesq approximation in Darcy model to study the double-diffusive natural convective flow in a shallow porous enclosure. Shirvan et al. [8] have examined the effect of MHD mixed convective heat transfer in a ventilated square cavity. It is found that the rate of heat transfer decreased with an increase in Hartmann number. Oztop [9] conducted a numerical study to investigate the mixed convection in a porous cavity with partially heated wall. He investigated an isothermal heater location on mixed convection flow and heat transfer. Chamkha [10] examined a numerical study to investigate the effect of magnetic field with combined convection flow in a vertical lid-driven cavity under the internal heat generation or absorption. His results showed that the flow characteristics behaviour inside the cavity are strongly affected by the influence of magnetic field. Few researchers, Chamkha and Abu-Nada [11], Tiwari and Das [12], and Nasrin et al. [13] performed numerical studies utilizing nanofluids to enhance heat transfer with mixed convection in lid-driven enclosures. Their results show that the Richardson number plays a vital role on the heat transfer characterization. In all these analysis, vertical walls are considered in motion. Khanafer and Chamka [14] analyzed on mixed convective flow in a lid-driven porous cavity. They found significant effect on the features of the temperature patterns and slight effects on the flow contours for small values of the Richardson number in presence of the internal heat generation. In [15], Basak et al. observed the effect of different thermal boundary conditions on mixed convection in a square enclosure filled with porous medium, It is found that at low Darcy number (Da = 10^{-5}), the heatlines are parallel and smooth for all values of Gr, Pr andRe. Thickness of the thermal boundary layer decreases along the side walls with increase in Da (Da = 10^{-3}) for larger Pr at low Re and Symmetric distribution in heatlines is observed. The influence of lid driven has been observed at higher Re, irrespective of Da and the thermal boundary layer is confined to the bottom and left wall as observed from packed heatlines. Sivakumar et al. [16] numerically observed the influence of heating size and location on mixed convection in driven enclosure. Sivasankaran et al. [17] also examined the mixed convection in a square cavity with nonuniform heating on left and right walls. They found that heat transfer rate is enhansed on increasing the ratio of amplitude and combined convection flow and heat transfer in a lid-driven square cav-

***Corresponding Author: B. M.D. Hidayathulla Khan,** Department of Mathematics, JNTU Ananthapur, Anantapuramu-515 002, India, E-mail: bmdhkh@gmail.com
V. Ramachandra Prasad, Department of Mathematics, Madanapalle Institute of Technology and Science, Madanapalle-517 325, India
R. Bhuvana Vijaya, Department of Mathematics, JNTU Ananthapur, Anantapuramu-515 002, India

ity filled with fluid saturated porous medium with nonuniform temperature distribution on both vertical walls was analysed by Sivasankaran et al. [18]. Rahman et al. [19] reported a numerical study of mixed convection flow in a channel with a fully or partially heated cavity in presence of magnetic field effect. It was found that the flow velocity decreases with increase in Hartmann number, and this reduces heat transfer and flow strength. Few of the researchers studied thermal radiation in detail [22–25].

In this article, mixed convection flow in a porous enclosure with effect of Radiation numerically using MAC method, in which both top and bottom walls are kept constant with cold temperature has been studied. The left and right walls are partially heated remaining portions are adiabatic. Obtained numerical results are presented graphically for stream functions and isotherms as well as the Nusselt number.

2 Physical model and Mathematical formulation

The schematic description of the problem along with no-slip thermal boundary conditions has been shown in Fig. 1. It is a square enclosure with L = H. The square cavity filled with porous medium having partially heated left and right walls and uniform cold temperature horizontal walls. The flow is considered to be 2D, laminar and incompressible. Density of the buoyancy forces is formulated by Boussinesq approximation. The Rosseland approximation [20] is used to describe the radiative heat flux in the energy equation.

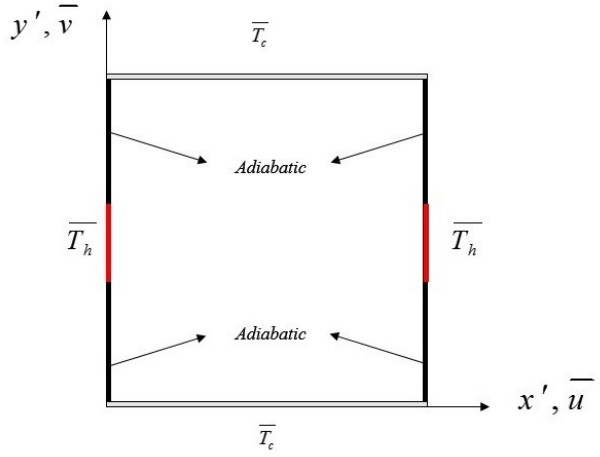

Fig. 1: Schematic diagram of flow configuration

The unsteady laminar 2D conservative partial differential equations of momentum and energy in Cartesian system can be written in dimensional form as follows:

$$\frac{\partial \bar{u}}{\partial x'} + \frac{\partial \bar{v}}{\partial y'} = 0 \tag{1}$$

$$\frac{\partial \bar{u}}{\partial t'} + \bar{u}\frac{\partial \bar{u}}{\partial x'} + \bar{v}\frac{\partial \bar{u}}{\partial y'} = -\frac{1}{\rho}\frac{\partial \bar{p}}{\partial x'} + \upsilon\left(\frac{\partial^2 \bar{u}}{\partial x'^2} + \frac{\partial^2 \bar{u}}{\partial y'^2}\right) - \frac{\upsilon}{k}\bar{u} \tag{2}$$

$$\frac{\partial \bar{v}}{\partial t'} + \bar{u}\frac{\partial \bar{v}}{\partial x'} + \bar{v}\frac{\partial \bar{v}}{\partial y'} = -\frac{1}{\rho}\frac{\partial \bar{p}}{\partial y'} + \upsilon\left(\frac{\partial^2 \bar{v}}{\partial x'^2} + \frac{\partial^2 \bar{v}}{\partial y'^2}\right) - \frac{\upsilon}{k}\bar{v} + \beta g\,(T - T_c) \tag{3}$$

$$\frac{\partial \bar{T}}{\partial t'} + \bar{u}\frac{\partial \bar{T}}{\partial x'} + \bar{v}\frac{\partial \bar{T}}{\partial y'} = \alpha\left(\frac{\partial^2 \bar{T}}{\partial x'^2} + \frac{\partial^2 \bar{T}}{\partial y'^2}\right) - \frac{1}{\rho c_p}\frac{\partial q_r}{\partial y'} \tag{4}$$

where $\alpha = \frac{k}{\rho c_p}$, we introduce the following non-dimensional variables

$$t = \frac{t' U_0}{L}, x = \frac{x'}{L},\ y = \frac{y'}{L},\ u = \frac{\bar{u}}{U_0},\ v = \frac{\bar{v}}{U_0},$$
$$p = \frac{\bar{p}}{\rho {U_0}^2},\ T = \frac{\bar{T} - \bar{T}_c}{\bar{T}_h - \bar{T}_c}$$

The radiation heat flux q_r is taken by Rosseland approximation [20] such that

$$q_r = -\frac{4\sigma}{3k^*}\frac{\partial \bar{T}^4}{\partial y'} \tag{5}$$

where σ and k^* are the Stefan-Boltzmann constant and the mean absorption coefficient. We assume that the differences in temperature within the flow are sufficiently small such that $\bar{T}^4$ can be described as a linear combination of the temperature. This is accomplished by expanding $\bar{T}^4$ in a Taylor series about $\bar{T}_c$ and neglecting higher order terms, then

$$\bar{T}^4 \cong 4\bar{T}_c^3\bar{T} - 3\bar{T}_c^4$$

and

$$\frac{\partial q_r}{\partial y'} = -\frac{16\sigma \bar{T}_c^3}{3k^*}\frac{\partial^2 \bar{T}}{\partial y'^2} \tag{6}$$

Utilizing Eq. (6), the Eqs. (1)- (4) transformed to

$$\frac{\partial u}{\partial x} + \frac{\partial v}{\partial y} = 0 \tag{7}$$

$$\frac{\partial u}{\partial t} + u\frac{\partial u}{\partial x} + v\frac{\partial u}{\partial y} = -\frac{\partial p}{\partial x} + \frac{1}{Re}\left(\frac{\partial^2 u}{\partial x^2} + \frac{\partial^2 u}{\partial y^2}\right) - \frac{1}{ReDa}u \tag{8}$$

$$\frac{\partial v}{\partial t}+u\frac{\partial v}{\partial x}+v\frac{\partial v}{\partial y}=-\frac{\partial p}{\partial y}+\frac{1}{\mathrm{Re}}\left(\frac{\partial^2 v}{\partial x^2}+\frac{\partial^2 v}{\partial y^2}\right)-\frac{1}{\mathrm{Re}\,Da}v+\frac{Gr}{\mathrm{Re}^2}T \tag{9}$$

$$\frac{\partial T}{\partial t}+u\frac{\partial T}{\partial x}+v\frac{\partial T}{\partial y}=\frac{1}{\mathrm{Re}\ \mathrm{Pr}}\left(\frac{\partial^2 T}{\partial x^2}+\frac{\partial^2 T}{\partial y^2}\right)+\frac{4}{3Nr}\frac{1}{\mathrm{Re}\ \mathrm{Pr}}\frac{\partial^2 T}{\partial y^2} \tag{10}$$

Here Gr is the Grashof number, Pr is the Prandtl number, Re is the Reynolds number and Nr is the Radiation parameter, which are defined as

$$\mathrm{Re}=\frac{U_0 L}{\upsilon},\ Da=\frac{k}{L^2},\ Nr=\frac{kk^*}{4\sigma\bar{T_c}^3},$$
$$Gr=\frac{g\beta\left(T_h-T_c\right)L^3}{\upsilon^2},\ \mathrm{Pr}=\frac{\upsilon}{\alpha}$$

Where the non-dimensional quantities x and y are the varying along horizontal and vertical directions respectively, u and v are corresponding directional velocities, T is the temperature of the fluid and p is the pressure.

The boundary conditions of the problem are described as follows:

On the top wall

$$y=1,\ 0<x<1,\ u=v=0,\ T=0$$

On the bottom wall

$$y=0,\ 0<x<1,\ u=v=0,\ T=0$$

On the left wall

$$x=0,\ 0<y<1, u=v=0,$$
$$T=\begin{cases}\frac{\partial T}{\partial x}=0\,,\ for\ 0<y<\frac{L}{4}\\ T=1,\quad for\ \frac{L}{4}<y<\frac{3L}{4}\\ \frac{\partial T}{\partial x}=0\,,\ for\ \frac{3L}{4}<y<1\end{cases}$$

On the right wall

$$x=1,\ 0<y<1, u=v=0,$$

$$T=\begin{cases}\frac{\partial T}{\partial x}=0\,,\ for\ 0<y<\frac{L}{4}\\ T=1,\quad for\ \frac{L}{4}<y<\frac{3L}{4}\\ \frac{\partial T}{\partial x}=0\,,\ for\ \frac{3L}{4}<y<1\end{cases} \tag{11}$$

The fluid motion is expressed using the stream function ψ evaluated from velocity components u and v as follows [21]

$$u=\frac{\partial\psi}{\partial y}\ \text{and}\ v=-\frac{\partial\psi}{\partial x}$$

One of the most physical quantities, the heat transfer coefficient in terms of the local Nusselt number (Nu) is defined by

$$Nu=-\frac{\partial T}{\partial n}$$

The average Nusselt number of each wall is defined by

$$AvgNu=\int_0^1 Nu_b dx,\ AvgNu=\int_0^1 Nu_t dx$$
$$AvgNu=\int_0^1 Nu_L dy,\ AvgNu=\int_0^1 Nu_R dy$$

3 Mac Numerical Solution and Validation

The momentum and energy balance equations (8)–(10) with conditions (11) have been solved using the MAC (Marker and Cell) Method (Amsden and Harlow 1970). The pressure distribution is obtained by making use of continuity equation (7). The numerical solutions are carried out in terms of the velocity components (u, v) and stream functions (ψ) . As per the Cauchy-Riemann equations, stream function (ψ) is defined as $u=\frac{\partial\psi}{\partial y}$ and $v=-\frac{\partial\psi}{\partial x}$ where positive and negative signs of ψ denotes anti-clockwise and clockwise circulations respectively. In the MAC approach although we consider viscous flow, viscosity is not actually required for numerical stability (Amsden and Harlow 1970). Cell boundaries are labelled with half-integer values in the finite difference discretization. The marker particles do not participate in the calculation. Here we elaborate on the numerical discretization procedure. Based on the weak conservative form of the unsteady two-dimensional Navier-Stokes equations and heat conservation equation as defined by eqns. (1)–(4), we implement a grid meshing procedure using the following notation at the centre of a cell:

$$u_{i-1/2,j}=\frac{1}{2}\left[u_{i-1,j}+u_{i,j}\right] \tag{12}$$

Applying to the x-direction momentum conservation Eq. (8) we have:

Discretized Advection terms:

$$\frac{\partial(uu)}{\partial x}=\frac{uu1-uu2}{\Delta x} \tag{13}$$

where

$$uu1=\left[\tfrac{1}{2}\left(u_{i,j}+u_{i+1,j}\right)\right]^2$$
$$uu2=\left[\tfrac{1}{2}\left(u_{i-1,j}+u_{i,j}\right)\right]^2 \tag{14}$$

Similarly, we have:

$$\frac{\partial(uv)}{\partial y}=\frac{uv1-uv2}{\Delta y} \tag{15}$$

where

$$uv1=\tfrac{1}{2}\left(u_{i,j}+u_{i,j+1}\right).\tfrac{1}{2}\left(v_{i,j}+v_{i+1,j}\right)$$
$$uv2=\tfrac{1}{2}\left(u_{i,j}+u_{i,j-1}\right).\tfrac{1}{2}\left(v_{i,j-1}+v_{i+1,j-1}\right) \tag{16}$$

The following central difference formula is used for the second order derivatives:

$$\nabla^2 u = \frac{\partial^2 u}{\partial x^2} + \frac{\partial^2 u}{\partial y^2}$$

$$\nabla^2 u = \frac{u_{i-1,j} - 2u_{i,j} + u_{i+1,j}}{\Delta x^2} + \frac{u_{i,j-1} - 2u_{i,j} + u_{i,j+1}}{\Delta y^2} \quad (17)$$

Applying to the *y*-direction momentum conservation Eq. (9) we have:

Advection term:

$$\frac{\partial(vu)}{\partial x} = \frac{vu1 - vu2}{\Delta x} \quad (18)$$

Here the following notation applies:

$$\begin{aligned} uv1 &= \tfrac{1}{2}\left(u_{i,j+1} + u_{i,j}\right).\tfrac{1}{2}\left(v_{i,j} + v_{i+1,j}\right) \\ uv2 &= \tfrac{1}{2}\left(u_{i-1,j+1} + u_{i-1,j}\right).\tfrac{1}{2}\left(v_{i,j} + v_{i-1,j}\right) \\ \tfrac{\partial(vv)}{\partial y} &= \tfrac{vv1 - vv2}{\Delta y} \end{aligned}$$

$$\begin{aligned} vv1 &= \left[\tfrac{1}{2}\left(v_{i,j+1} + v_{i,j}\right)\right]^2 \\ vv2 &= \left[\tfrac{1}{2}\left(v_{i,j-1} + v_{i,j}\right)\right]^2 \end{aligned} \quad (19)$$

The central difference formula for the Laplacian operator is given by:

$$\begin{aligned} \nabla^2 v &= \tfrac{\partial^2 v}{\partial x^2} + \tfrac{\partial^2 v}{\partial y^2} \\ \nabla^2 v &= \tfrac{v_{i-1,j} - 2v_{i,j} + v_{i+1,j}}{\Delta x^2} + \tfrac{v_{i,j-1} - 2v_{i,j} + v_{i,j+1}}{\Delta y^2} \end{aligned} \quad (20)$$

Effectively the *x*-momentum equation discretization technique can be summarized as:

$$\widetilde{u} = u^n + dt.\left[-\left(u\frac{\partial u}{\partial x} + v\frac{\partial u}{\partial y}\right) + \alpha_1\left(\frac{\partial^2 u}{\partial x^2} + \frac{\partial^2 u}{\partial y^2}\right) - \alpha_2 u\right] \quad (21)$$

where $\alpha_1 = {}^1/_{\mathrm{Re}}$, and $\alpha_2 = {}^1/_{\mathrm{Re}.Da}$. There is a slight modification needed in the *y*-momentum equation due to the addition of a new term. Therefore this term must be included in the discretized equation and we have:

$$\widetilde{v} = v^n + dt.\left(-\left[u\frac{\partial v}{\partial x} + v\frac{\partial v}{\partial y}\right] + \alpha_1\left(\frac{\partial^2 v}{\partial x^2} + \frac{\partial^2 v}{\partial y^2}\right) - \alpha_2 v + \beta.T\right) \quad (22)$$

where $\alpha_1 = {}^1/_{\mathrm{Re}}$, $\alpha_2 = {}^1/_{\mathrm{Re}.Da}$ and $\beta = {}^{Gr}/_{\mathrm{Re}^2}$. It is further noteworthy that the temperature term T is co-located such that it coincides with velocity before using it in the above equation to account for the staggered grid. After $\widetilde{u}$ and $\widetilde{v}$ are projected to get u and v by Poisson pressure equation

$$\frac{\nabla.u^*}{dt} = \nabla^2 p$$

we can use the discretized temperature equation to get T at next time level (T^{n+1}) via the algorithm:

$$T^{n+1} = T^n + \Delta t.\left[-\left(u\frac{\partial T}{\partial x} + v\frac{\partial T}{\partial y}\right) + \chi\left(\frac{\partial^2 T}{\partial x^2} + \frac{\partial^2 T}{\partial y^2}\right)\right] \quad (23)$$

where $\chi = \frac{1}{\mathrm{Re\,Pr}}$. Next, we integrate in time by an incremental step dt in each iteration until the final time $t = 1.0$ is reached. The variables are co-located and plotted. Modern variants of the MAC method utilize the conjugate gradient schemes which solve the Poisson equation. Further details are provided in Amsden and Harlow (1970). To confirm mesh independence a grid-independence study is conducted. In computational fluid dynamics, we adopt different methods for simulation, among which finite difference simulation is merely one methodology. Once a mesh provides a solution which is invariant with the finer meshes, the coarser mesh can be adopted. This reduces computational cost but retains the necessary accuracy. Table 1 shows that accuracy up to three decimal places is achieved for Nusselt number at the left wall with a mesh of 61 × 61 which is sufficient for heat transfer computations and therefore this is adopted for all subsequent simulations.

Table 1: Grid independent study

Grid size	Average Nusselt number (Nu)
21 × 21	0.1500
31 × 31	0.1525
41 × 41	0.1554
51 × 51	0.1587
61 × 61	0.1592

Furthermore to corroborate the present computations, temperature (isotherms) and streamline distributions for two special cases have been visualized. These replicate the solutions of Kandaswamy *et al.* (2008). The equivalent Rayleigh number used in (Kandaswamy et al. 2008) is merely the product of the thermal Grashof number and Prandtl number, which has been considered as Rayleigh number (i.e. *Ra = Gr Pr*) in present study. Generally very close correlation is attained, as observed in Figs. 2 and 3 and confidence in the present MAC computational code is therefore justifiably high.

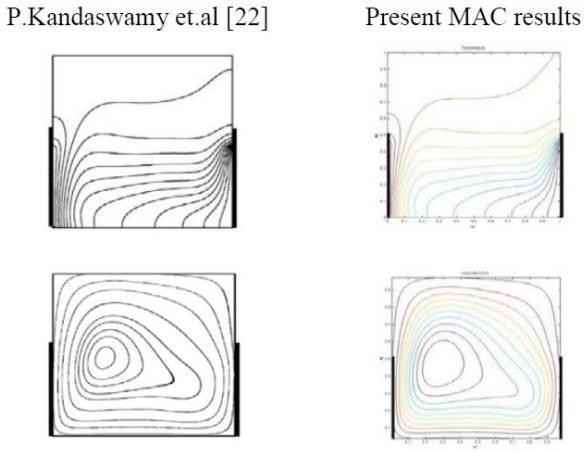

Fig. 2: .Comparison contour plots, for bottom-bottom thermal condition vertical walls with $Pr = 0.71$, $Gr = 10^5$, $Ha = 10$

4 Results and Discussion

In this section, results of mixed convection in an enclosure filled with porous medium have been discussed. The horizontal walls of the enclosure are kept at constant temperature (cold temperature) while the two vertical walls are partially heated and the rest of the wall portions are thermally insulated. The working fluid is chosen as air with Prandtl number Pr = 0.71 and is fixed throughout the study. Numerical results of streamlines and isotherms for various values of governing flow parameters such as Radiation parameter Nr, thermal Grashof number (Gr), Darcy number (Da) and Reynolds number (Re) presented graphically. The values of flow parameters are $Nr = 1$, Pr = 0.71 and Re = 10 considered by default unless specified. The numerical computations are performed for $Ri > 1$ and $Da \geq 0.001$, a remarkable changes in isotherms and stream function patterns.

Fig. 3A-C shows the influence of Radiation on the flow patterns and isotherms for$Gr = 10^3$, Re = 10 and for varying Darcy parameter $\left(Da = 10^{-3} - 10^{-1}\right)$. The streamlines are formed in two circulation cells which occupy equal space in the cavity and these circulations are formed along active portion of the thermal wall is observed. The isotherms are smoothly increasing from heated location and are symmetric.

Fig. 4A-C illustrates the transient results of isotherms and streamlines for $Gr = 10^4$, Re = 10, $Nr = 1$ and for varying Darcy parameter $\left(Da = 10^{-3} - 10^{-1}\right)$. Flow circulation cells are appeared near the hot region is activated. If Da is increased the primary circulation cell decreases. Half of the cavity is occupied by the primary circulation

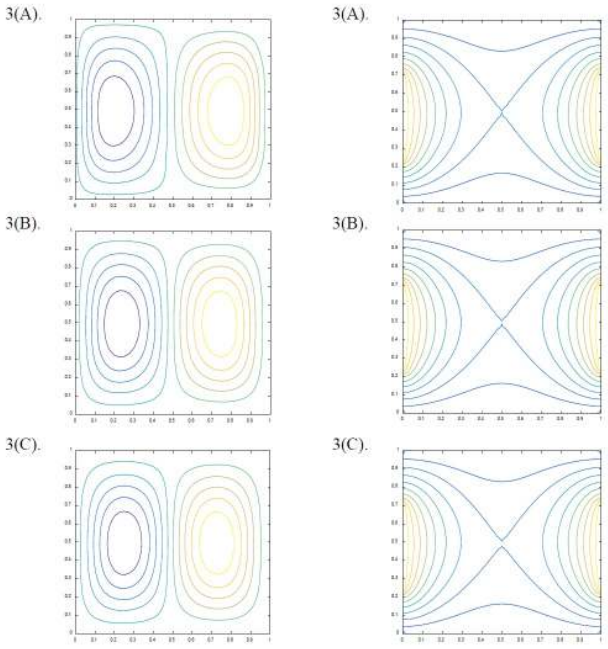

Fig. 3: Streamlines and Isotherms for $Nr = 1$, $Gr = 10^3$, $Pr = 0.71$, (A) $Da = 0.001$, (B) $Da = 0.01$, (C) $Da = 0.1$

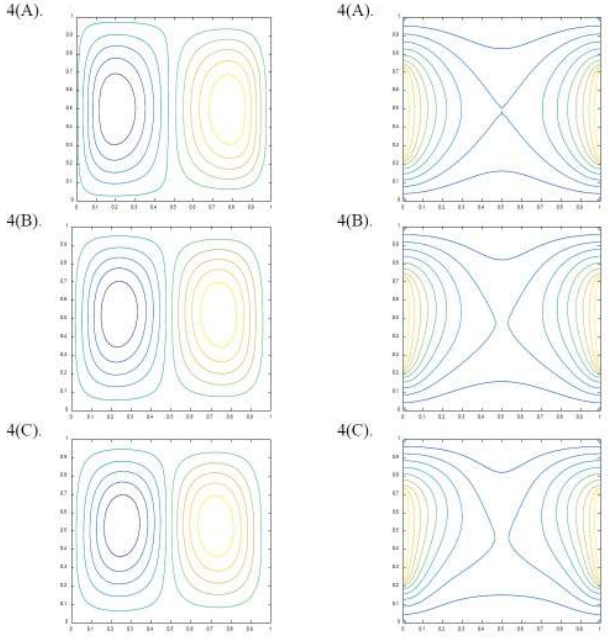

Fig. 4: Streamlines and Isotherms for $Nr = 1$, $Gr = 10^4$, $Pr = 0.71$, (A) $Da = 0.001$, (B) $Da = 0.01$, (C) $Da = 0.1$

cell and another half by the secondary circulation cell and these circulation cells are formed vertically. The isotherms are distributed within the cavity from the active heating portion of the side walls. The strength of the isotherms re-

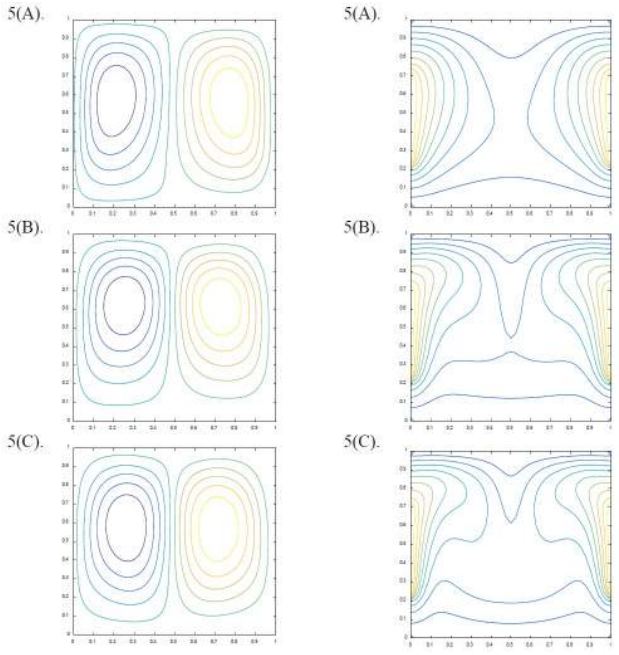

Fig. 5: Streamlines and Isotherms for $Nr = 1$, $Gr = 10^5$, $Pr = 0.71$, (A) $Da = 0.001$, (B) $Da = 0.01$, (C) $Da = 0.1$

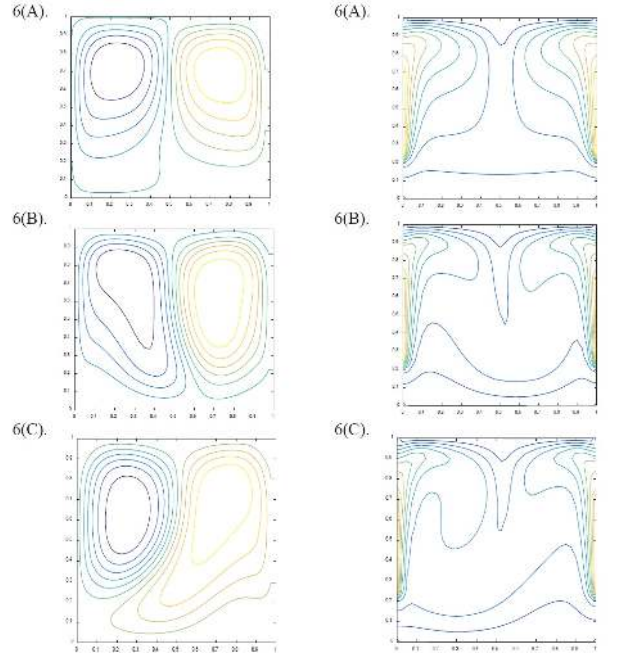

Fig. 6: Streamlines and Isotherms for $Nr = 1$, $Gr = 10^6$, $Pr = 0.71$, (A) $Da = 0.001$, (B) $Da = 0.01$, (C) $Da = 0.1$

duces from the heating part to middle of the cavity, the effects are reflected in both opposite active portions.

Fig. 5A-C shows the streamlines and isotherms for $Gr = 10^5$, Re $= 10$, $Nr = 1$ and for varying Darcy parameter $\left(Da = 10^{-3} - 10^{-1}\right)$. The isotherms appear to be distorted at the cold top wall of the cavity where as they become hyperbolic shaped near the hot side of the active portions, the similar patterns of isotherms are examined at $Gr = 10^4$. The symmetric circulation cells are appeared near side walls of the square enclosure, also left circulation cell is bigger than the right circular circulation cell for all values of Da. Dense isotherm patterns are appeared near the top cold wall with enhanced Da. The wavy shaped isotherms formed near the cold bottom wall for low $Da = 10^{-3}$, the wavy shape of isotherms near bottom wall smoothly changes for increasing value of Da.

The transient results of streamlines and isotherms are depicted in Fig. 6A-C, for governing parameters $Gr = 10^6$, Re $= 10$, $Nr = 1$ and for varying Darcy parameter $\left(Da = 10^{-3} - 10^{-1}\right)$. The effect of Radiation is observed for various values of Da, the magnitude of streamlines is very low signifying dominant conduction heat transfer is observed. Symmetric circulation cells diminish gradually for increase in Darcy parameter Da and also the circulation cells shape is gradually changed. The isotherms are compressed towards the cold top wall whereas the dense isotherms are gradually disappear in centre of the cavity and isotherms are almost symmetric. It is observed that the streamlines stretch diagonally for two cases one is $Da = 10^{-2}$ and another one is for high $Da = 10^{-1}$. The thermal boundary layer is formed gradually at heating portions for increased Da.

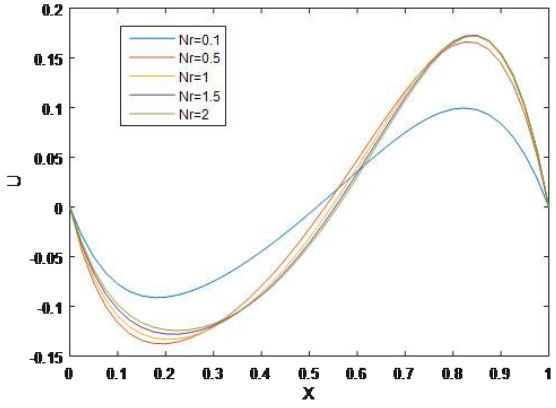

Fig. 7: Central line velocity of U for various Nr values with $Re = 10$, $Pr = 0.71$, $Gr = 10^4$, $Da = 0.1$

Figure 7 represents the mid-plane u-velocity due to Radiation effect. The velocities change their direction as the Radiation increases. The mid-plane u-velocity increases and then reaches back to zero for enhanced Radiation parameter (Nr). The Radiation effect on central line v-velocity of a square cavity filled with porous medium has been shown in Figure 8. The mid-plane v-velocity gradually re-

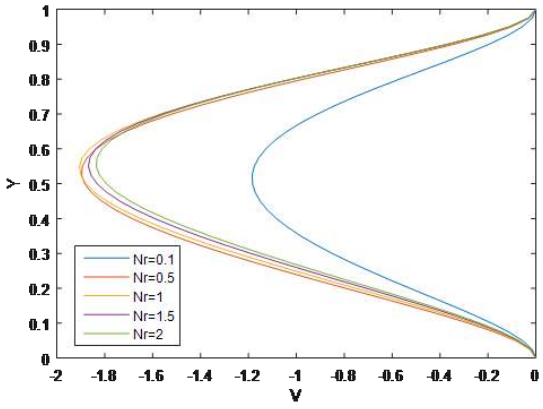

Fig. 8: Central line velocity of V for various Nr values with $Re = 10$, $Pr = 0.71$, $Gr = 10^4$, $Da = 0.1$

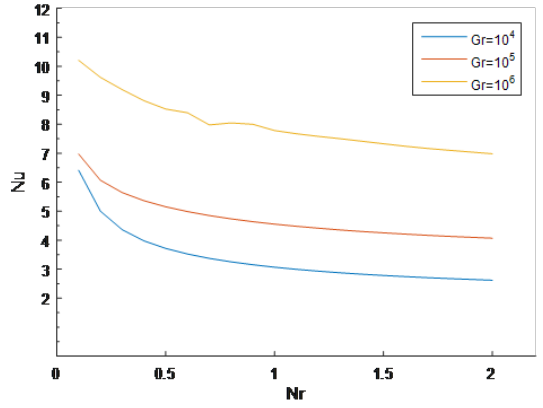

Fig. 9: Average Nusselt Number for different Gr values with $Re = 10$, $Pr = 0.71$, $Da = 0.1$

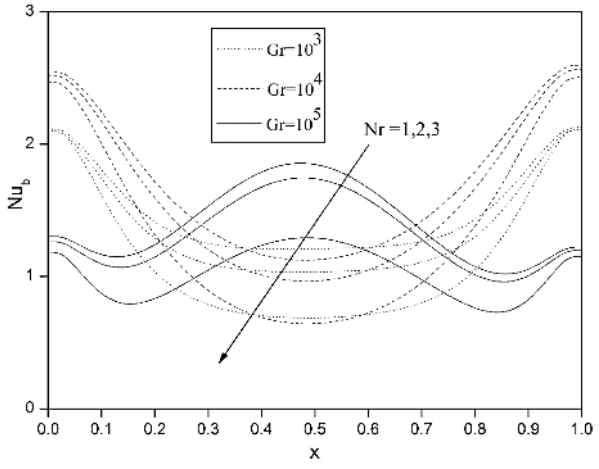

Fig. 10: Local Nusselt Number of bottom wall for different Gr values and various Nr values with $Re = 10$, $Pr = 0.71$, $Da = 0.1$

duces with increase in Radiation parameter (Nr). The aver-

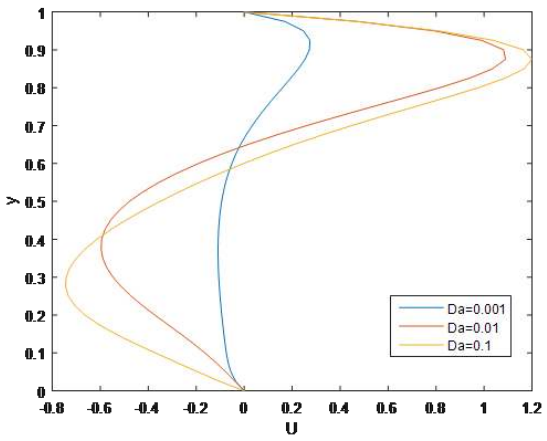

Fig. 11: Central line velocity of U for various Da values with $Re = 10$, $Pr = 0.71$, $Gr = 10^5$, $Nr = 0$

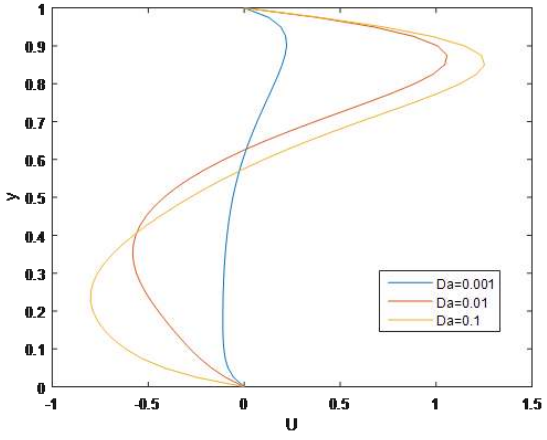

Fig. 12: Central line velocity of U for various Da values with $Re = 10$, $Pr = 0.71$, $Gr = 10^5$, $Nr = 1$

age Nusselt Number (Nu) varies with respect to Radiation parameter (Nr) and Grashof number (Gr) at the left vertical wall depicted in Figure 9. The average Nusselt number (Nu) is reduced with an increase in Grashof number (Gr). The influence of Grashof number (Gr) on local Nusselt number at the bottom wall with varying Radiation parameter (Nr) has been observed in Figure 10 with fixed $Re = 10$, $Pr = 0.71$ and $Da = 0.1$, the heat transfer in the middle of the bottom wall is slowly increased with an increase in the Grashof number (Gr). Figure 11–13 shows the variation of mid-velocity U for different Darcy numbers in presence of Radiation, the velocity is having sinusoidal nature except the absence of Radiation, the velocity is enhanced with increasing Da.

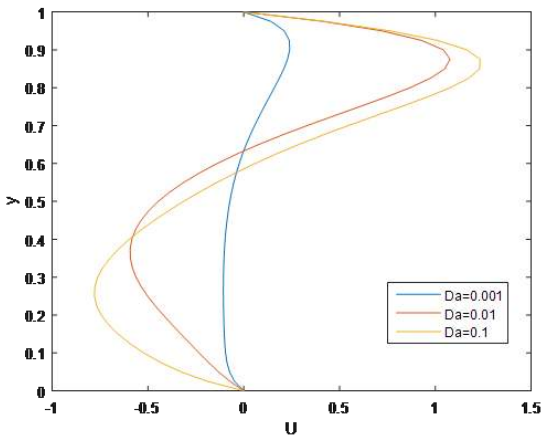

Fig. 13: Central line velocity of U for various Da values with $Re = 10$, $Pr = 0.71$, $Gr = 10^5$, $Nr = 2$

5 Conclusions

The numerical study has been analysed on mixed convection in porous square cavity with central heating of vertical walls under thermal Radiation. The non-dimensional governing parameters that influence the flow and heat transfer characteristics are Grashof Number, Reynolds Number and Radiation Parameter. In view of the computed results, the following findings can be drawn to make a summary as:

1. The heat transfer increases with an increase in the Grashof number. Thus, Grashof number plays an important role to control heat transfer and fluid flow.
2. The heat transfer increases with increasing of Darcy number for high values of Grashof number, the Darcy number plays a vital role to control fluid flow and heat transfer.
3. Thermal radiation parameter increases with an increase in heat transfer for all values of Grashof number. The convection is controlled by thermal Grashof number.
4. The flow and temperature contours are affected with Grashof number and thermal radiation. The local heat transfer enhancement is observed as the thermal radiation increases.

In the present study we consider Newtonian fluid flow with thermal Radiation in porous media within a square enclosure. Furthermore, we study the similar effect on micro polar regime in different geometries like triangular, skewed and wavy surface enclosures.

References

[1] A. F. Khudheyer, MHD mixed convection in double lid-driven differentially heated trapezoidal cavity, International Journal of Application or Innovation in Engineering and Management, 2015, vol. 4.

[2] GH.R. Kafayati, M.G. Bandpy, H. Sajjadi, and D. D. Ganji, Lattice Boltzmann simulation of MHD mixed convection in a lid-driven square cavity with linearly heated wall, Scientia Iranica B, 2012, vol. 19, pp. 1053-1065.

[3] A. Chattopadhyay, S. K. Pandit, S. S. Sarma, and I. Pop, Mixed convection in a double lid-driven sinusoidally heated porous cavity, International Journal of Heat and Mass Transfer, 2016, vol. 93, pp. 361-378.

[4] H. Moumni, H. Welhezi, R. Djebali, and E. Sediki, Accurate fnite volume investigation of nanouid mixed convection in two-sided lid driven cavity including discrete heat sources," Applied Mathematical Modelling, 2015,vol. 39, pp. 4164-4179.

[5] A. Malleswaran, S. Sivasankaran, and M. Bhuvaneswari, Effect of heating location and size on MHD mixed convection in a lid-driven cavity, International Journal of Numerical Methods for Heat and Fluid Flow, 2013, vol. 23, pp. 867-884.

[6] M. H. Esfe, M. Akbari, A. Karimipour, M. Afrand, O. Mahian, and S. Wongwises, Mixed convection ow and heat transfer in an inclined cavity equipped to a hot obstacle using nanofluids considering temperature-dependent properties, International Journal of Heat and Mass Transfer, 2015, vol. 85, pp. 656-666.

[7] Kalla, L., Vasseur, P., Benacer, R., Beji, H., and Duval, R. Double diffusive convection within a horizontal porous layer salted from the bottom and heated horizontally. International communications in heat and mass transfer, 2001, vol. 28(1), pp.1-10.

[8] K. M. Shirvan, M. Mamourian, S. Mirzakhanlari, and M. Moghiman, Investigation on effect of magnetic field on mixed convection heat transfer in a ventilated square cavity, Procedia Engineering, 2015, vol. 127, pp. 1181-1188.

[9] Oztop, H.F., Combined Convection Heat Transfer in a Porous Lid-Driven Enclosure due to Heater with Finite Length, *Int. Comm. Heat Mass Transfer,* 2006, 33 (6), pp.772–779.

[10] Chamkha, A., Hydromagnetic Combined Convection Flow in a Vertical Lid-Driven Cavity with Internal Heat Generation or Absorption, *Numerical Heat Transfer, Part A,* 2002, 41(5), pp.529-546.

[11] A.J. Chamkha, E. Abu-Nada, Mixed convection flow in a single and double lid driven square cavities filled with water-Al2O3 nanofluid: effects of viscosity models, Eur. J. Mech. B-Fluid, 2012, 36, 82–96.

[12] R.K. Tiwari, M.K. Das, Heat transfer augmentation in a two-sided lid-driven differentially heated square cavity utilizing nanofluids, Int. J. Heat Mass Transfer, 2007, 50, 2002–2018.

[13] R. Nasrin, A.J. Chamkha, M.A. Alim, Modeling of mixed convective heat transfer utilizing nanofluid in a double lid-driven chamber with internal heat generation, Inter. J. Numer. Method Heat Fluid Flow, 2014, 24, 36–57.

[14] K. Khanafer, A.J. Chamkha, Mixed convection flow in a lid-driven enclosure filled with a fluid-saturated porous medium, Int. J. Heat Mass Transfer, 1999, 42, 2465–2481.

[15] T. Basak, P.V.K. Pradeep, S. Roy, I. Pop, Finite element based heat line approach to study mixed convection in a porous

square cavity with various wall thermal boundary conditions, Int. J. Heat Mass Transfer, 2011, 54 (9-10) , 1706–1727.

[16] V. Sivakumar, S. Sivasankaran, P. Prakash, J. Lee, Effect of heating location and size on mixed convection in lid-driven cavity, Comput. Math. Appl., 2010, 59, 3053–3065.

[17] S. Sivasankaran, V. Sivakumar, P. Prakash, Numerical study on mixed convection in a lid-driven cavity with non-uniform heating on both side walls, Int. J. Heat Mass Transfer, 2010, 53 ,4304–4315.

[18] S. Sivasankaran, K.L. Pan, Numerical simulation on mixed convection in a porous lid-driven cavity with non-uniform heating on both side wall, Numer. Heat Transfer Part A, 2012, 61, 101–121.

[19] Rahman, M.M.; Öztop, H.F.; Saidur, R.; Mekhilef, S.; Al-Salem, K.: Finite element solution of MHD mixed convection in a channel with a fully or partially heated cavity. Comput. Fluids, 2013, 79, 53–64.

[20] W.M. Rohsenow, J.P. Hartnett, Y.I. Cho(eds). Handbook of Heat Transfer. 3rd ed. *New York*, *McGraw-Hill,* (1998).

[21] G.K. Batchelor, An introduction to fluid dynamics, Cambridge University Press, 1993.

[22] Sameh E. Ahmed, Ahmed Kadhim Hussein, H.A. Mohammed, I.K. Adegun, Viscous Dissipation and radiation effects on MHD natural convection in a square enclosure filled with porous medium, *Nuclear Engineering and Design*, 2014, 266, 34-42.

[23] Tapas Ray Mahapatra, Dulal Pal, Sabyasachi Mondal, Mixed Convection flow in an inclined enclosure under magnetic field with thermal radiation and heat generation, *International Communications in Heat and Mass Transfer,* 2013, 41, 47-56.

[24] G.Palani, K.Y.Kim, Influence of Magnetic field and thermal radiation by natural convection past vertical cone subjected to variable surface heat flux, *Applied Mathematics and Mechanics,* English Edition, 2012, 33(5), 605-620.

[25] Tapas Ray Mahapatra, Dulal Pal, Sabyasachi Mondal, Natural Convection in a Lif-driven square cavity filled with Darcy-Forchheimer porous medium in the presence of thermal radiation, *International Journal of Nonlinear Science,* 2011, 11(3), 366-379.